PHYSICAL REVIEW C **87**, 014617 (2013)

# Monte Carlo Hauser-Feshbach predictions of prompt fission $\gamma$ rays: Application to $n_{th} + {}^{235}U$, $n_{th} + {}^{239}Pu$, and ${}^{252}Cf$ (sf)

B. Becker,[1] P. Talou,[2,*] T. Kawano,[2] Y. Danon,[1] and I. Stetcu[2]

[1]*Gaerttner LINAC Laboratory, Rensselaer Polytechnic Institute, New York 12180, USA*

[2]*T-2 Nuclear Theory Group, Los Alamos National Laboratory, Los Alamos, New Mexico 87545, USA*

(Received 14 August 2012; revised manuscript received 6 December 2012; published 28 January 2013)

The prompt neutron and $\gamma$ emission from primary fission fragments are calculated for thermal neutron induced fission of ${}^{235}U$ and ${}^{239}Pu$ and for spontaneous fission of ${}^{252}Cf$ using a Monte Carlo Hauser-Feshbach approach for the evaporation of the excited fission fragments. Remaining free model parameters, such as excitation energy sharing and initial spin distribution, are determined by comparison of the neutron emission characteristics with experimental data. Using the obtained parameters the $\gamma$-ray characteristics, e.g., $\gamma$ spectrum, multiplicity distribution, average multiplicity and energy, and multiplicity distribution, are calculated and compared with available experimental data.

DOI: 10.1103/PhysRevC.87.014617 PACS number(s): 25.85.Ec, 24.75.+i, 24.10.Lx

## I. INTRODUCTION

The prompt particle emission from primary fission fragments right after scission is the primary mechanism of the de-excitation of the fission fragments. Both the excitation energy and angular momentum are reduced by the emission of neutrons and $\gamma$ rays. The characteristics of the emitted particles, such as their multiplicity and energy distribution, contain valuable information for our understanding of the pre- and postscission physics. In particular, they provide information on the excitation energy sharing and angular momentum distribution near the point of separation of the two fragments.

In the past, several Monte Carlo tools have been developed to simulate the particle emission based on sequential emission from the excited fission fragments [1–8]. They all share the same techniques based on a Weisskopf evaporation spectrum for the emissions of prompt neutrons. $\gamma$ rays have been considered only as a byproduct of the final stage of the decay where the excitation energy was not sufficient to cause neutron emission. More recently, Litaize and Serot [6] have introduced a slightly more accurate description of the neutron-$\gamma$ competition, albeit in a phenomenological correction to the Weisskopf-type approach only.

In the present paper, we replace the commonly used Weisskopf evaporation spectrum with a Monte Carlo Hauser-Feshbach approach that simulates the evaporation of prompt neutrons and $\gamma$ rays in competition. By comparing the calculated neutron emission characteristics with experiments, the remaining free model parameters are determined. Using these model parameters, the $\gamma$ emission of the fission fragments can be predicted. The particles emitted from thermal neutron induced fission of ${}^{235}U$ and ${}^{239}Pu$ and of spontaneous fission of ${}^{252}Cf$ are calculated and compared to various experiments.

In Sec. II the Hauser-Feshbach model and its Monte Carlo implementation are described. In Sec. III we discuss the initial, preparticle emission properties of the fission fragments. Numerical results for $n_{th} + {}^{235}U$, $n_{th} + {}^{239}Pu$, and ${}^{252}Cf$ (sf) are discussed in Secs. IV–VI, respectively.

## II. MONTE CARLO APPROACH TO FISSION FRAGMENT EVAPORATION

The general concept of a Monte Carlo approach to calculate the evaporation of particles from fission fragments has been discussed at length in several previous publications [2,9]. In this work we recall the basic elements of this approach and discuss the improvements made by replacing the Weisskopf evaporation model by a full Hauser-Feshbach calculation.

### A. Sampling of the fission fragment decay path

The starting point of each Monte Carlo sampling of the evaporation process is always the primary fission fragment distribution formed after scission but before neutron emission. The initial state of a fragment is fully defined by its initial mass $A$, charge $Z$, spin $J$, parity $\pi$, excitation energy (XE), and kinetic energy (KE). It is further assumed that particles are only emitted from fully accelerated fission fragments.

The sampling of the initial states of the light and the heavy fragment is performed in several steps. First, we introduce the mass and total kinetic energy (TKE) dependent preneutron emission fragment yield matrix $Y(A, \mathrm{TKE})$ (see Sec. III A). This matrix is used to sample directly TKE and the mass of the heavy fragment $A_h$. The mass of the complementary light fragment is then obtained by $A_l = A_c - A_h$, where $A_c$ is the mass of the fissioning nucleus. Once fragment masses and TKE are determined, the charge, spin and parity are sampled according to several models (see Secs. III B and III D). Then, the total excitation energy TXE is calculated and shared between both fragments (Sec. III C). Starting from these well defined initial conditions, neutrons and $\gamma$ rays are emitted sequentially until the excitation energies of both fragments are fully dissipated. Properties of emitted particles such as multiplicity, kinetic energy and emission angle are recorded for every fission event. Average quantities such as the average

*Corresponding author: talou@lanl.gov

 

neutron multiplicity $\overline{\nu}_n(A, \mathrm{TKE})$, or correlated and exclusive quantities such as the exclusive spectrum for a given neutron multiplicity $\chi(E_{\mathrm{out}})_{|\nu=n}$, the $\gamma$ multiplicity distribution $P(N_\gamma)$, the average $\gamma$ multiplicity as a function of mass and TKE, $\overline{N}_\gamma(A, \mathrm{TKE})$, etc., can be calculated.

The Monte Carlo decay code FFD (fission fragment decay) was coupled with the Monte Carlo Hauser-Feshbach code CGM. FFD is used to sample the initial fission fragments and to perform the analysis of simulated histories while CGM calculates the particle emission from specific fragments.

### B. Neutron evaporation using a Weisskopf model

Following the approach of Weisskopf [10], the neutron emission is simulated by sampling an evaporation spectrum at temperature $T$ given by

$$\rho(\epsilon_n) = \epsilon_n \exp(-\epsilon_n / T_{A-1,Z}), \tag{1}$$

where $\epsilon_n$ is the kinetic energy of the neutron in the center-of-mass reference frame. $T_{A-1,Z}$ is the temperature of the residual nucleus $(A-1, Z)$, given by

$$T_{A-1,Z} = \sqrt{\frac{U(A,Z) - S_n(A,Z)}{a_{A-1,Z}}}, \tag{2}$$

where $a_{A-1,Z}$ is the level density parameter of the residual nucleus, and $S_n$ and $U_{A,Z}$ are the neutron separation and excitation energy, respectively. The residual nucleus is formed with an excitation energy of

$$U_{A-1,Z} = U_{A,Z} - S_n - \epsilon_n. \tag{3}$$

In addition, the sampling of the neutron energy is constrained by $\epsilon_n < U_{A,Z} - S_n$. At some point the residual excitation energy becomes small enough such that neutron emission is not energetically possible. In previous publications that use this methodology [2,3,6] the sequential neutron emission is terminated at an excitation energy limit above the neutron binding energy in order to account roughly for the competition between neutron and $\gamma$ emissions.

### C. Hauser-Feshbach model

In the Weisskopf approximation, the spin and parity of the intermediary excited states are ignored, and only the energy of the system is conserved. On the contrary, in the Hauser-Feshbach statistical theory [11], energy, spin and parity of the nuclear states follow specific conservation rules. We have implemented a Monte Carlo Hauser-Feshbach (MCHF) code, called CGM [12], which has been used to obtain the numerical results discussed below.

In this approach, the probabilities of emitting prompt $\gamma$ rays and prompt neutrons are calculated simultaneously as follows:

$$P(\epsilon_\gamma)d\epsilon_\gamma \propto T_\gamma(\epsilon_\gamma)\rho(Z, A, U - \epsilon_\gamma), \tag{4}$$

and

$$P(\epsilon_n)d\epsilon_n \propto T_n(\epsilon_n)\rho(Z, A-1, U - \epsilon_n - S_n). \tag{5}$$

The energy-dependent neutron transmission coefficients $T_n(\epsilon_n)$ are calculated using the optical model potential of Koning and Delaroche [13], while the $\gamma$-ray transmission coefficients $T_\gamma(\epsilon_\gamma)$ are obtained in the strength function formalism, with default parameters taken from the Reference Input Parameter Library RIPL-3 database [14].

The level density $\rho(U)$ is represented in the Gilbert-Cameron formalism [15], with a constant temperature behavior at the lowest excitation energies and a Fermi gas representation at higher energies, taking into account the washing-out of shell effects with increasing excitation energy. The spin and parity dependence of the level density are given as

$$\rho(U, J, \pi) = \tfrac{1}{2}\rho(U) f(J, U), \tag{6}$$

with

$$f(J, U) \propto (2J+1)\exp\left\{-\frac{J(J+1)}{2\sigma^2(U)}\right\}, \tag{7}$$

where $\sigma^2$ is the spin cut-off parameter of the level density.

The parameters for the Gilbert-Cameron representation of the level density were taken from RIPL-3 [14]. Discrete levels and decay branching ratios in the discrete region were also taken from RIPL-3, and are mostly based on the ENSDF nuclear structure database.

## III. PRIMARY FISSION FRAGMENT DISTRIBUTIONS

The complete initial fission fragment yield distribution $Y(A, Z, \mathrm{TKE}, J, \pi)$ is given as a function of mass $(A)$, charge $(Z)$, total kinetic energy (TKE), spin $(J)$, and parity $(\pi)$. As mentioned in the previous section in this work the initial fragment yield distribution is decomposed into several partial distributions:

$$Y(A, Z, \mathrm{TKE}, J, \pi) = Y(A, \mathrm{TKE})P(Z|A)P(J, \pi|A), \tag{8}$$

where $Y(A, \mathrm{TKE})$ is the mass and TKE dependent fragment yield, $P(Z|A)$ is the normalized charge distribution for a specific mass, and $P(J, \pi|A)$ is the normalized, mass-dependent spin and parity distribution, in which it is assumed that $P(\pi) = 1/2$ in the continuum. These partial distributions are either based on introduced experimental data or on specific models.

### A. Mass and total kinetic energy distribution

Two different approaches are used for the mass and TKE dependent fragment yield $Y(A, \mathrm{TKE})$. For $n_{\mathrm{th}} + {}^{235}\mathrm{U}$ and ${}^{252}\mathrm{Cf}$ (sf) we directly used experimental data measured with double sided Frisch-grid ionization chambers [16,17]. For $n_{\mathrm{th}} + {}^{239}\mathrm{Pu}$ the matrix $Y(A, \mathrm{TKE})$ is reconstructed by using partial data of the mass dependent yield $Y(A)$ and the mass-dependent mean total kinetic energy $\langle \mathrm{TKE} \rangle(A)$ as well as its standard deviation $\sigma_{\mathrm{TKE}}(A)$. Specific details on how $Y(A, \mathrm{TKE})$ was obtained in the case of $n_{\mathrm{th}} + {}^{239}\mathrm{Pu}$ can be found in Ref. [7]. Figures 1 and 2 show the yield matrix of $n_{\mathrm{th}} + {}^{235}\mathrm{U}$ and $n_{\mathrm{th}} + {}^{239}\mathrm{Pu}$, respectively.

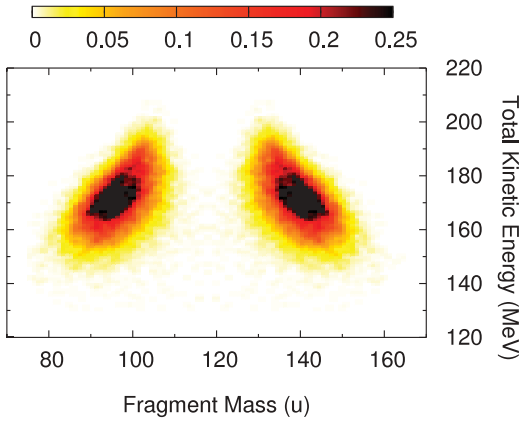


FIG. 1. (Color online) Primary fission fragment yields as a function of mass and total kinetic energy for $n_{\rm th} + {}^{235}$U, as measured by Romano *et al.* [16]. The units of the color scale are in percent. The yield is normalized to 200%.

### B. Charge distribution

The normalized charge distribution $P(Z|A)$ for a given mass $A$ is obtained using Wahl systematics [18]. For every heavy mass, the charge deviation $\Delta Z$, the charge width parameter $\sigma_Z$, and the odd-even factors $F_Z$ and $F_N$ are calculated. The charge distribution is then determined by using

$$P(Z|A) = \tfrac{1}{2} F(A) N(A) \left[\mathrm{erf}(V) - \mathrm{erf}(W)\right], \tag{9}$$

with

$$V = \frac{Z - Z_p + 0.5}{\sigma_Z \sqrt{2}} \quad \text{and} \quad W = \frac{Z - Z_p - 0.5}{\sigma_Z \sqrt{2}}, \tag{10}$$

and the normalization factor $N(A)$. The most probable charge is given by

$$Z_p = A_h \frac{Z_c}{A_c} + \Delta Z, \tag{11}$$

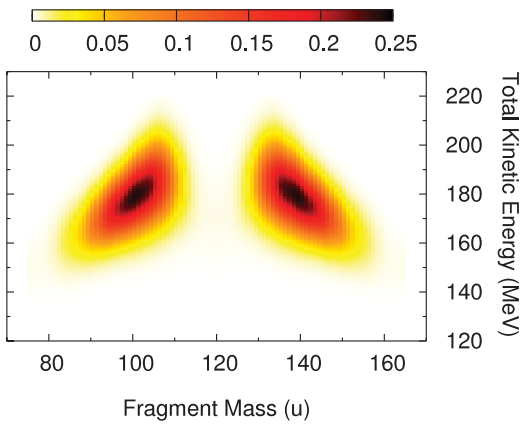


FIG. 2. (Color online) Same as Fig. 1 but for $n_{\rm th} + {}^{239}$Pu. The units of the color scale are in percent. The yield is normalized to 200%. Contrary to Fig. 1, this plot was obtained by computing the yields directly from Eq. (8).

where $Z_c$ is the charge of the fissioning nucleus. The odd-even factor $F(A)$ is calculated as

$$\begin{aligned} F(A) &= F_Z \times F_N && \text{for } Z \text{ even and } N \text{ even}, \\ F(A) &= F_Z / F_N && \text{for } Z \text{ even and } N \text{ odd}, \\ F(A) &= F_N / F_Z && \text{for } Z \text{ odd and } N \text{ even}, \\ F(A) &= 1/(F_Z \times F_N) && \text{for } Z \text{ odd and } N \text{ odd}. \end{aligned}$$

The charge of the light fragment is simply inferred by $Z_l = Z_c - Z_h$.

### C. Excitation energy sharing

For a given pair of fission fragments, the total excitation energy TXE to be shared among the light and heavy fragments is given by

$$\begin{aligned} \mathrm{TXE} &= Q_f(A_l, Z_l; A_h, Z_h) - \mathrm{TKE} \\ &= M_n(A_l, Z_l) + M_n(A_h, Z_h) - M_n(A_c, Z_c) \\ &\quad + E_{\rm inc} + B_n(A_c, Z_c) - \mathrm{TKE}, \end{aligned} \tag{12}$$

where $Q_f$ is the $Q$ value of the fission reaction, and $M_n$ represent the nuclear masses of the light $(A_l, Z_l)$ and heavy $(A_h, Z_h)$ fragments, and of the fissioning nucleus $(A_c, Z_c)$. $E_{\rm inc}$ is the incident neutron energy and $B_n$ is the neutron binding energy of the fissioning nucleus.

The total excitation energy (TXE) is shared between the two fragments using the $R_T$ parameter [19], which is defined as the ratio of the initial fragment temperatures:

$$R_T = T_0^l / T_0^h, \tag{13}$$

where $T_0^l$ and $T_0^h$ are the initial temperatures in the light and heavy fragment. This initial temperature ratio is translated into a ratio of the initial excitation energies of the fragments using the Fermi-gas relation. $R_T = 1.0$ represents the state of thermal equilibrium between the two nascent fragments used in the original Los Alamos model [20]. In this work we use two different approaches for $R_T$: (i) either $R_T$ is set to an average constant value or (ii) $R_T$ is mass-dependent and inferred by minimizing the discrepancy between calculated and experimental values of $\overline{\nu}_l/\overline{\nu}_h$ as a function of the heavy fragment mass $A_h$. For the latter approach, a series of Monte Carlo calculations using the Weisskopf evaporation model was done with different mass independent values for $R_T$ resulting in a matrix of $\overline{\nu}_l/\overline{\nu}_h$ as function of $R_T$ and $A_h$. In similar manner as done in Ref. [7], a polynomial fit of $R_T(A_h)$ was determined which minimizes the discrepancy between calculated and experimental values of $\overline{\nu}_l/\overline{\nu}_h$. Figure 3 shows $\overline{\nu}_l/\overline{\nu}_h$ using $R_T = 1.2$ and the obtained $R_T(A)$ for $n_{\rm th} + {}^{235}$U. The behavior of $R_T(A)$ follows closely $\overline{\nu}_l/\overline{\nu}_h$. At symmetry, $R_T$ should be equal to 1.0 as there is no distinction between light and heavy fragments. Then $R_T$ rises sharply culminating slightly below $A_h = 130$ which corresponds to the decrease in excitation energy in the heavy fragments near spherical closed shell. In turn, very few neutrons are emitted from the heavy fragment. As we move toward more asymmetric configurations, $R_T$ decreases and eventually becomes less than 1.0. In this case, nuclear shape calculations [21] show that the heavier fragment becomes more deformed than its

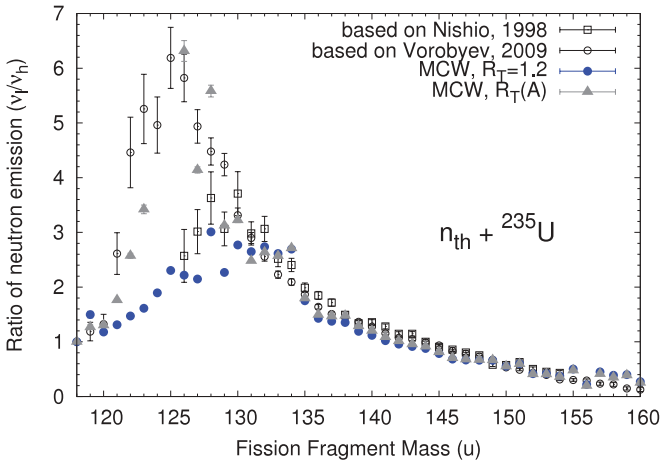


FIG. 3. (Color online) $\overline{\nu}_l/\overline{\nu}_h$ as a function of the heavy fragment mass using $R_T = 1.2$ and $R_T(A)$. $R_T(A)$ was obtained by minimizing the discrepancies of the calculated ratio and of the experimental data of Nishio *et al.* [23] and Vorobyev *et al.* [24].

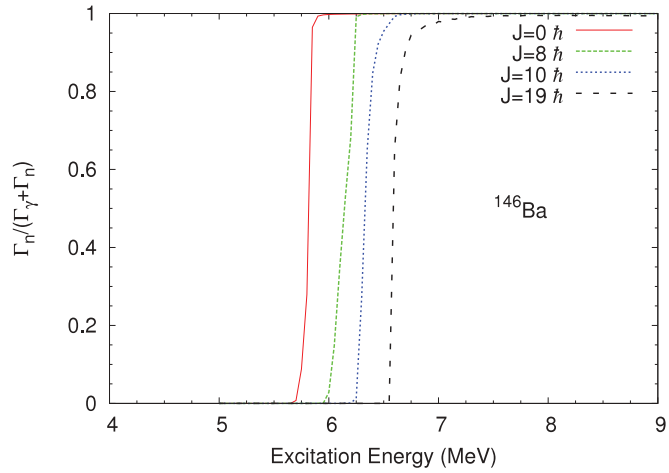


FIG. 4. (Color online) Neutron emission probability $\Gamma_n/(\Gamma_n + \Gamma_\gamma)$ as a function of the excitation energy for different spin values for $^{146}$Ba.

light partner. The deformation energy being transformed into intrinsic excitation energy right after scission therefore explains that $R_T$ falls below unity. Similar approaches to derive $R_T$ have been done by Litaize and Serot [6] and by Manailescu *et al.* [22].

### D. Spin and parity distribution

In our study we assume that the spin of the primary fission fragments has the same functional form as the angular momentum distribution of the nuclear level density as in Eq. (7),

$$P(J|A) \sim (2J+1)e^{-\frac{J(J+1)}{B^2}}, \tag{14}$$

where $B$ acts a spin cut-off parameter for the initial fission fragment spin distribution. Note that $B \sim J_{\rm rms}$ and that $B$ is a free parameter in our model and not necessarily equivalent to $\sqrt{2}\sigma$ in Eq. (7).

We consider three cases: (i) $B$ is a constant and does not depend on the fragment mass, (ii) the initial spin cut-off parameter has a saw-tooth like behavior, and (iii) $B$ is a function of the fragment temperature $T$, mass $A$ and the ground state deformation $\beta$.

In the second case we use an approach similar to Mouze *et al.* [25] who proposed a saw-tooth like behavior for the initial spin distribution as function of the fragment mass. The initial spin of the fragment masses $A = 82$ and $A = 126$ are assumed to be zero corresponding to spherical shell closures. In order to maintain a distribution for the initial spin we assume a saw-tooth like behavior of the cut-off parameter $B(A)$. The slopes of the saw tooth are adjusted in order to obtain the best agreement of the average neutron multiplicity $\overline{\nu}_{\rm tot}$ with evaluated library data.

Following Ericson [26], in the third case we assume a dependence of the initial spin distribution on the fragment temperature, mass, and deformation:

$$B^2(T, A, \beta) \propto \frac{\mathcal{J}(T, A, \beta)T}{\hbar^2}, \tag{15}$$

where $\mathcal{J}$ is the moment of inertia of the nucleus. In this study we use deformation-dependent rigid body moment of inertia $\mathcal{J}_{\rm rig}(A, \beta)$ neglecting any temperature dependence. The deformation-dependent rigid body moment of inertia $\mathcal{J}_{\rm rig}(A, \beta)$ is

$$\mathcal{J}_{\rm rig}(A, \beta) = \tfrac{2}{5} A m_n R^2 (1 + 0.31\beta + 0.44\beta^2 + \cdots), \tag{16}$$

where $\beta$, $m_n$, $R$ are the quadrupole deformation parameter, the nucleon mass, and the fragment radius ($R = 1.15A^{1/3}$ fm), respectively. In principle the quadrupole deformation parameter should be taken from the fragment at the time of emission, however here we make the approximation of using the quadrupole deformation parameter of the nucleus at ground state taken from RIPL-3 [14]. The absolute magnitude of $B(T, A, \beta)$ represents an additional free parameter in our model and is chosen according to the best agreement of $\overline{\nu}_{\rm tot}$ with evaluated library data. Of course in return this means that $\overline{\nu}_{\rm tot}$ cannot be considered as an outcome of the simulation.

Several constant spin cut-off parameters are investigated in this work ranging form 6 to 12$\hbar$. As mentioned before, by replacing the Weisskopf-spectrum with a MCHF calculation the neutron-$\gamma$ competition is introduced. This competition is strongly dependent on the fission fragment spin (Fig. 4). For low spin values, the ratio $\Gamma_n/(\Gamma_n + \Gamma_\gamma)$ is nearly a step function with a transition from 0 to 1 at excitation energies close to the neutron separation energy $S_n$. For higher spin values the probability of a $\gamma$ emission increases at the expense of neutron emission probability.

Table I summarizes the fixed input and corresponding references. The model parameters and the observables used to constrain them are given as well.

## IV. RESULTS FOR $n_{\rm th} + ^{235}$U

The decay of fission fragments from $n_{\rm th} + ^{235}$U was simulated. We first discuss the differences of the calculated neutron data using either Weisskopf (MCW) or Hauser-Feshbach (MCHF) models. Then we address the results obtained for

TABLE I. Main input parameters, free model parameters and observable used to constrain the free parameters.

| Fixed input | | Reference |
|---|---|---|
| Fragment yield | $Y(A, \mathrm{TKE})$ | [7,16,17] |
| Charge distribution | $P(Z\|A)$ | [18] |
| Neutron separation energies | $S_n$ | [27] |
| Level densities | $\rho, a$ | [14] |
| $\gamma$-ray transmission coefficients | $T_\gamma(\epsilon_\gamma)$ | [14] |
| Model parameter | | Observable used to constrain parameter |
| Excitation energy sharing | $R_T$ | $\nu_l/\nu_h(A_h)$ |
| Initial spin distribution | $B$,$B(A)$, $B(T, A, \beta)$ | $\overline{\nu}_{\mathrm{tot}}$ |

the $\gamma$-particle emission obtained with the Hauser-Feshbach model.

Note that all plotted or given uncertainties of the calculations are purely due to the stochastic nature of the Monte Carlo simulations. They do not represent a full uncertainty estimation since important uncertainties of of model or input quantities such as the fission fragment yields were not considered.

### A. Prompt fission neutron multiplicity (PFNM)

The average neutron multiplicity was calculated using Weisskopf and Hauser-Feshbach models (Table II). Several trends can be observed by performing MCW calculations. Using a higher excitation energy limit for neutron emission ($E^*_{\mathrm{limit}}$), i.e., $S_n + \delta$ instead of $S_n$, where $\delta$ is an effective threshold energy shift simulating the $\gamma$-neutron competition as observed in Fig. 4, leads to a decrease of the total neutron multiplicity by about 0.3–0.4 neutrons per fission. As

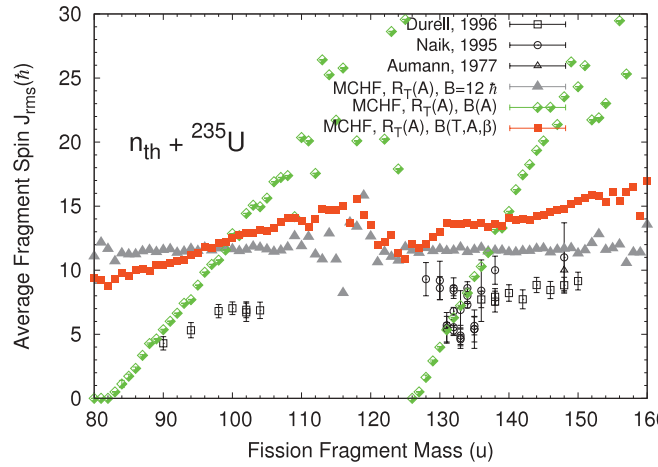


FIG. 5. (Color online) Average initial fission fragment spin for $n_{\mathrm{th}} + {}^{235}\mathrm{U}$ as a function of the fragment mass for MCHF calculations using a constant spin cutoff parameter $B = 12\hbar$, using a temperature, mass and ground state deformation dependent spin cutoff parameter and using a saw-tooth like spin cutoff parameter $B(A)$. Experimental values are taken from Durell (digitized from Ref. [25]), Naik *et al.* [29] and Aumann *et al.* [28].

expected, increasing $R_T$ increases the neutron emission from the light fragment at the expense of the emission from the heavy fragment. The use of a mass dependent $R_T$ parameter (see Sec. III C) instead of $R_T = 1.2$ changes the average light, heavy and total multiplicity only slightly since 1.2 is a rather good estimation of $R_T$ in the mass region with the highest yield.

The Monte Carlo Hauser-Feshbach calculations were done using either a constant value for the spin cut-off parameter ($B = 9\hbar$ or $B = 12\hbar$), using a saw-tooth like behavior of the spin cut-off parameter $B(A)$ or by using a temperature, mass and ground state deformation dependent spin cut-off parameter $B(T, A, \beta)$. By increasing the spin cutoff parameter

TABLE II. Average neutron multiplicity for $n_{\mathrm{th}} + {}^{235}\mathrm{U}$ of the light ($\overline{\nu}_l$) and heavy fragment ($\overline{\nu}_h$) and total average neutron multiplicity $\overline{\nu}_{\mathrm{tot}}$ for Weisskopf Spectrum (MCW) and Hauser-Feshbach (MCHF) based Monte Carlo calculations. Different model parameter assumptions were used for the excitation energy sharing parameter $R_T$, for the lower excitation energy limit $E^*_{\mathrm{limit}}$ in MCW calculations and for the spin cut-off parameter $B$ in MCHF calculations. $S_n$ is the neutron separation energy of the fission product, and $\delta$ is the energy shift used in MCW calculations to simulate the neutron-$\gamma$ competition.

| | $E^*_{\mathrm{limit}}$ | $B$ | $R_T$ | $\overline{\nu}_l$ | $\overline{\nu}_h$ | $\overline{\nu}_{\mathrm{tot}}$ |
|---|---|---|---|---|---|---|
| MCW | $S_n$ | – | 1.0 | 1.287 | 1.534 | $2.821 \pm 0.002$ |
| MCW | $S_n + \delta$ | – | 1.0 | 1.114 | 1.400 | $2.514 \pm 0.002$ |
| MCW | $S_n + \delta$ | – | 1.2 | 1.322 | 1.088 | $2.410 \pm 0.002$ |
| MCW | $S_n + \delta$ | – | $R_T(A)$ | 1.353 | 1.053 | $2.407 \pm 0.001$ |
| MCHF | – | $9\hbar$ | $R_T(A)$ | 1.456 | 1.130 | $2.586 \pm 0.003$ |
| MCHF | – | $12\hbar$ | $R_T(A)$ | 1.386 | 1.075 | $2.461 \pm 0.003$ |
| MCHF | – | $B(A)$ | $R_T(A)$ | 1.424 | 1.006 | $2.430 \pm 0.003$ |
| MCHF | – | $B(T, A, \beta)$ | $R_T(A)$ | 1.387 | 1.030 | $2.417 \pm 0.003$ |
| Nishio *et al.* [23] | | | | 1.42 | 1.01 | – |
| Holden [30] | | | | – | – | $2.430 \pm 0.007$ |
| Hopkins [31] | | | | – | – | $2.42 \pm 0.02$ |
| Zhang [32] | | | | – | – | $2.400 \pm 0.004$ |
| ENDF/B-VII.0 [33] | | | | – | – | 2.42 |

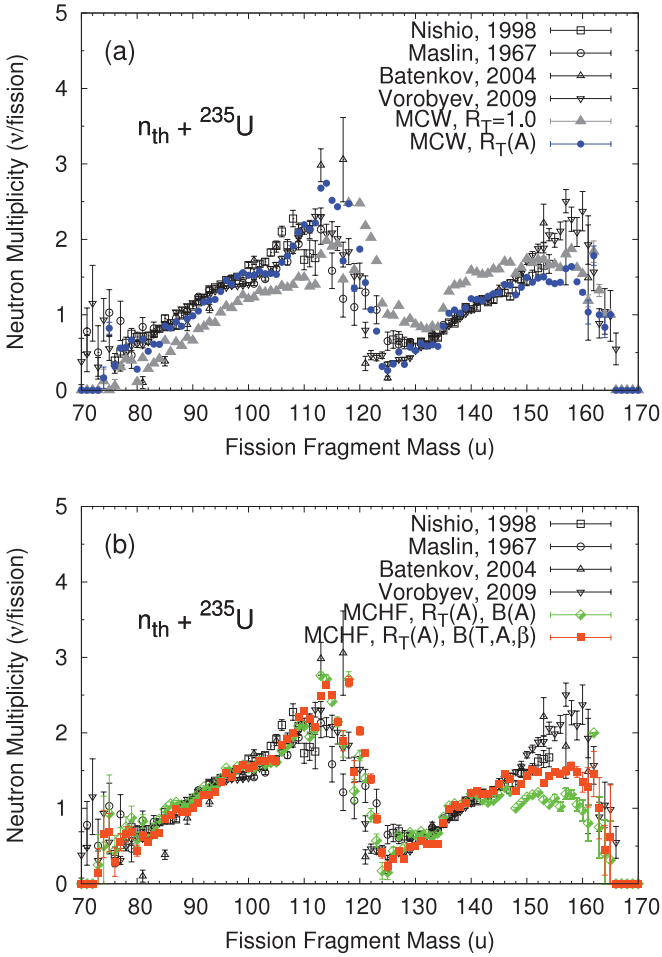


FIG. 6. (Color online) Average prompt fission neutron multiplicity (PFNM) for $n_{\text{th}} + {}^{235}\text{U}$ as a function of the fragment mass: (a) A constant value $R_T = 1.0$ as well as a the mass-dependent $R_T(A)$ parameter was used for the Monte Carlo Weisskopf Spectrum (MCW) calculations. (b) The Monte Carlo Hauser Feshbach (MCHF) calculation is obtained using a mass-dependent $R_T(A)$ parameter and a temperature, mass and ground state deformation dependent spin cutoff parameter $B$. Experimental values are taken from Nishio *et al.* [23], Maslin *et al.* [34], Batenkov *et al.* [35], and Vorobyev *et al.* [24].

the average neutron multiplicity decreases as $\Gamma_\gamma$ increases with higher spins. Figure 5 shows the average initial fragment spin using $B = 12\hbar$, $B(A)$ using $B(T, A, \beta)$ as a function of fission fragment mass. Even though all three cases lead to a good average neutron multiplicity $\overline{\nu}_{\text{tot}}$, the average initial spins are higher than the initial spins deduced from isomeric yield ratio experiments of Durell [25], Aumann *et al.* [28], and those compiled by Naik *et al.* [29].

Figure 6 shows the average neutron multiplicity as a function of the fission fragment mass. With a mass dependent $R_T$ parameter a very good agreement with the experimental data is found, except for masses greater than ∼145 u. One has to note however, that in case of using $R_T(A)$ the result for $\overline{\nu}(A)$ is not a pure outcome of the simulation since $R_T(A)$ is based on the $\overline{\nu}_l/\overline{\nu}_h(A)$ data (see Sec. III C). In this case, both the MCW and the MCHF calculations give approximately the same result for $\overline{\nu}(A)$. For masses above 145 u, $B(A)$ leads to a decrease of the multiplicity compared to $B(T, A, \beta)$ due to an increased initial fragment spin while experimental data points in the opposite direction.

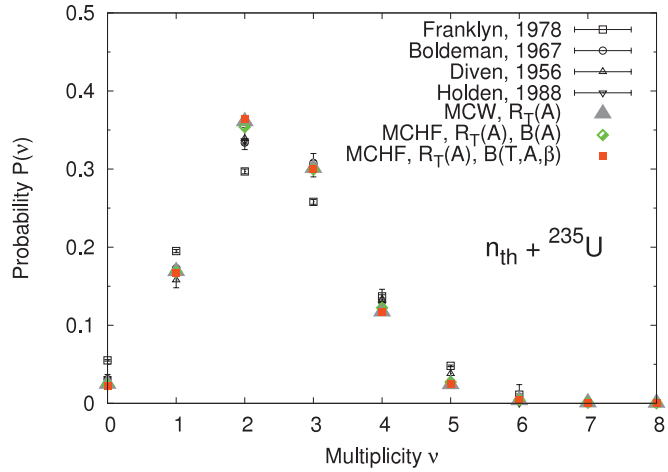


FIG. 7. (Color online) Neutron multiplicity distributions for $n_{\text{th}} + {}^{235}\text{U}$ obtained in Monte Carlo Weisskopf spectrum (MCW) and Monte Carlo Hauser-Feshbach (MCHF) calculations vs. the experimental data of Franklyn *et al.* [36], Boldeman *et al.* [37], Diven *et al.* [38], and Holden *et al.* [39].

The calculated neutron multiplicity distribution (Fig. 7) is in very good agreement with Holden's evaluation [39], slightly overpredicting $P(\nu = 2)$.

### B. Prompt fission neutron spectrum (PFNS)

The prompt fission neutron spectrum was evaluated using both Weisskopf and Hauser-Feshbach calculations.

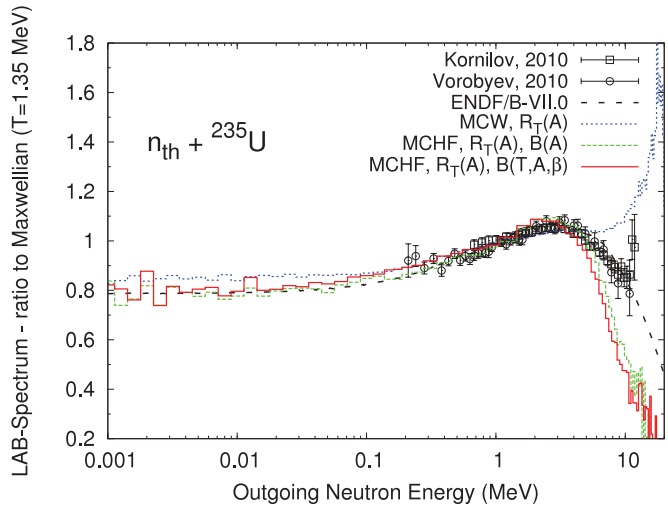


FIG. 8. (Color online) Average prompt fission neutron spectrum for $n_{\text{th}} + {}^{235}\text{U}$ in ratio to a Maxwellian with temperature $T = 1.35$ MeV. Those results were calculated based on a Weisskopf (MCW) and Hauser-Feshbach (MCHF) models using $R_T(A)$ and $B(T, A, \beta)$. Results are compared to the ENDF/B-VII.0 evaluation [33], as well as experimental data by Kornilov *et al.* [40] and Vorobyev *et al.* [41].

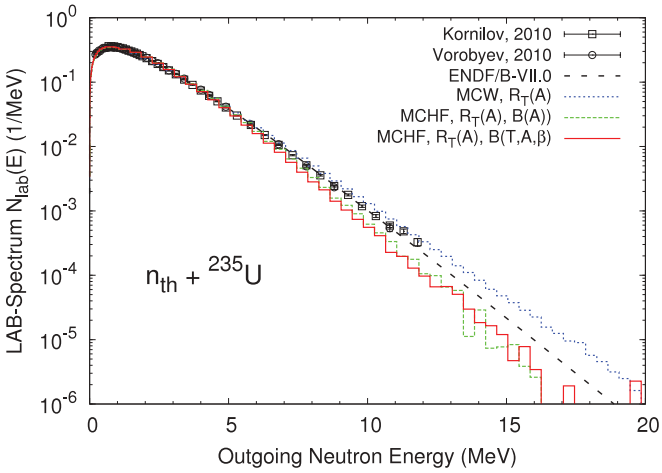


FIG. 9. (Color online) Same as Fig. 8, but plotted on an absolute scale.

The obtained spectra were compared to the ENDF/B-VII.0 evaluation [33] based on the Los Alamos model and to experimental data. The experimental data were normalized to the ENDF/B-VII.0 spectrum. Figure 8 shows the spectra as a ratio to a Maxwellian ($T = 1.35$ MeV), while Fig. 9 shows the absolute spectra. The low energy tail of both MCHF calculations agrees with he ENDF/B-VII.0 spectrum while the MCW caculation is higher. On the other hand, in the Weisskopf-based approach, the high-energy tail of the spectrum is harder than in the ENDF evaluation. A similar tendency was observed by Talou *et al.* [7] and Vogt *et al.* [8] for the calculated PFNS of $^{239}$Pu$(n, f)$. As pointed out by Talou *et al.* [7], the high-energy tail of the spectrum is very sensitive to the $R_T$ parameter. Using a mass dependent $R_T$ parameter instead of $R_T = 1.0$ tends to harden the spectrum. However, using a Hauser-Feshbach model, the spectrum is found to be softer than ENDF/B-VII.0 spectrum, as illustrated in Fig. 9. The main reason for this difference is found in the average neutron kinetic energy in the center of mass reference frame emitted from the light fragment (see Fig. 10). While for the heavy fragments all calculations give similar results, differences can be noticed for the light fragments. The average neutron energy calculated with the Hauser-Feshbach model is lower that the one calculated using Weisskopf spectra. For the light fragment MCHF calculations are in good agreement with the experimental values of Batenkov *et al.* [35] and Vorobyev *et al.* [24] while MCW are closer to the measurement of Nishio *et al.* [23]. For the heavy fragments all calculations are lower than the experimental results. Using a saw-tooth like $B(A)$ instead of $B(T, A, \beta)$ in a MCHF calculation slightly lowers the low energy tail of the neutron spectrum while increasing the high energy tail. Note that $\langle E_{\text{c.m.}} \rangle$ values are difficult to estimate experimentally, and rely on Maxwellian fits to mass-specific center-of-mass neutron spectra, as in Nishio *et al.* [23]. Significant systematic uncertainties can be expected from this approach.

### C. Average $\gamma$ multiplicity and energy

The Monte Carlo Hauser-Feshbach model was used to calculate average properties of the $\gamma$ emission such as the

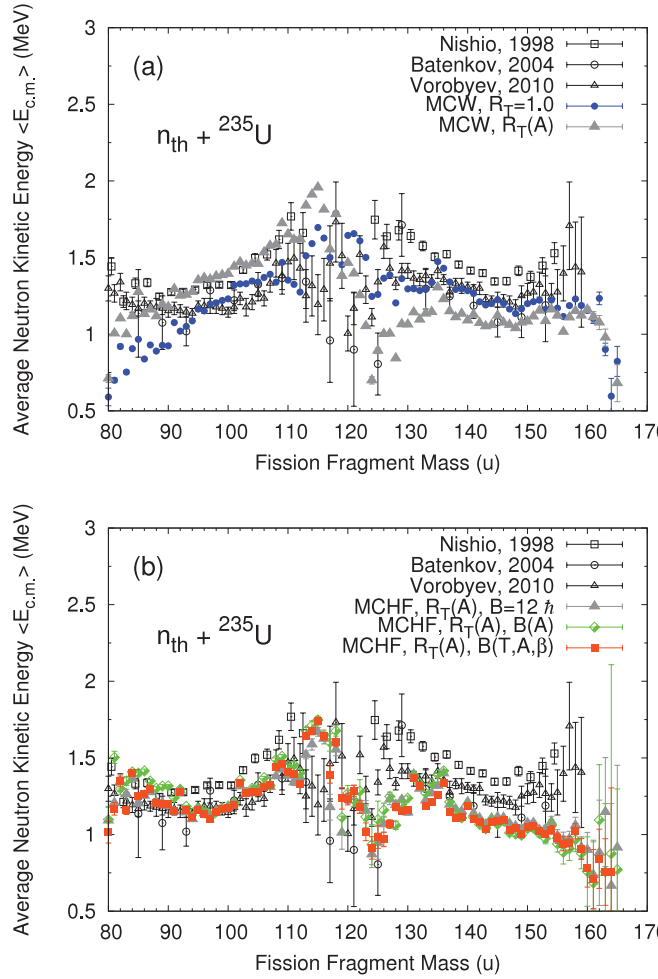


FIG. 10. (Color online) Average center-of-mass energy of the prompt fission neutrons for $n_{\text{th}} + ^{235}$U as a function of the fragment mass. (a) A constant value $R_T = 1.0$ as well as a mass-dependent $R_T(A)$ parameter were used for the Monte Carlo Weisskopf spectrum (MCW) calculations. (b) The Monte Carlo Hauser-Feshbach (MCHF) calculations were obtained using a mass-dependent $R_T(A)$ parameter and a temperature, mass and ground state deformation dependent spin cutoff parameter $B$. Experimental values are taken from Nishio *et al.* [23], Batenkov *et al.* [35], and Vorobyev [41].

$\gamma$ multiplicity and total and average $\gamma$ energy (Table III). An increase of the spin cut-off parameter and consequently of the average initial spin leads to an increase of $\gamma$ multiplicity and total $\gamma$ energy. The neutron-$\gamma$ competition is shifted towards $\gamma$ emission. In addition, the average $\gamma$ energy decreases with increasing initial spin. The higher the spin the more $\gamma$-rays are emitted along the yrast line with a relatively small energy.

The measured average $\gamma$ multiplicity depends strongly on the experimental energy threshold for $\gamma$ detection. In order to compare our calculated results with experiments a lower energy threshold of 140 keV is chosen. In addition, the experimental measured $\gamma$ multiplicity might depend on the time interval after a fission event open for $\gamma$ detection. The longer the time interval the more short-lived delayed $\gamma$ rays are detected. However, Pleasonton *et al.* [42] pointed out that

TABLE III. Average $\gamma$ multiplicity ($\overline{N}_\gamma$), average $\gamma$ energy ($\overline{\epsilon}_\gamma$), and average total $\gamma$ energy ($\overline{E}_\gamma$) for $n_{th} + {}^{235}$U. Monte Carlo Hauser-Feshbach (MCHF) calculations were obtained with either a constant, saw-tooth like [$B(A)$] or with a temperature, mass and ground state deformation dependent spin cut-off parameter [$B(T, A, \beta)$]. $\Delta E$ is the considered $\gamma$ energy range and $\Delta t$ the experimental $\gamma$ detection time range after fission. The bold lines indicate the most comparable calculation and measurement in terms of $\Delta t$, $\Delta E$, and obtained results.

| | $B$ [$\hbar$] | $\Delta E$ (MeV) | $\Delta t$ (ns) | $\overline{N}_\gamma$ [$\gamma$/fission] | $\overline{\epsilon}_\gamma$ [MeV/$\gamma$] | $\overline{E}_\gamma$ [MeV/fission] |
|---|---|---|---|---|---|---|
| MCHF | 9 | >0.14 | – | 6.25 | 0.95 | 5.94 |
| MCHF | 12 | >0.14 | – | 7.60 | 0.88 | 6.74 |
| MCHF | $B(A)$ | >0.14 | – | 7.80 | 0.88 | 6.86 |
| **MCHF** | $\boldsymbol{B(T, A, \beta)}$ | **>0.14** | – | **8.05** | **0.88** | **7.06** |
| MCHF | $B(T, A, \beta)$ | >0.01 | – | 10.89 | 0.66 | 7.19 |
| Verbinski *et al.* [43] | | 0.14–10.0 | 10 | $6.7 \pm 0.3$ | $0.97 \pm 0.05$ | $6.51 \pm 0.3$ |
| **Peelle** *et al.*. [47] | | **0.14–10.0** | **69** | $\mathbf{7.45 \pm 0.32}$ | **0.96*** | $\mathbf{7.18 \pm 0.26}$ |
| Peelle *et al.* [47] | | 0.01–10.5 | 69 | $8.13 \pm 0.35$ | 0.87[a] | $7.25 \pm 0.26$ |
| Rau (taken from [42]) | | 0.10–2.5 | 220 | $7.0 \pm 0.1$ | 1.20 | $9.5 \pm 0.2$ |
| Pleasonton *et al.* [42] | | 0.09–10.0 | 5 | $6.51 \pm 0.3$ | 0.99 | $6.43 \pm 0.3$ |
| Pleasonton *et al.* [42] | | 0.03–10.4 | 70 | $8.1 \pm 0.8$ | 0.90 | $7.0 \pm 0.7$ |
| Pleasonton *et al.* [42] | | 0.03–10.4 | 275 | $8.6 \pm 0.8$ | 0.86 | $7.4 \pm 0.7$ |
| ENDF/B-VII.0 [33] | | | | 7.0437 | | |
| JEFF-3.1 [48] | | | | 7.17 | | |
| JENDL-4.0 [49] | | | | 7.4283 | | |
| CENDL-3.1 [50] | | | | 8.095 | | |

[a]calculated using $\overline{\epsilon}_\gamma = \frac{\overline{E}_\gamma}{\overline{N}_\gamma}$.

a long time interval might lead to false counts due to neutron detections.

In our calculations we consider the full decay chain of the fission fragments. The calculated average $\gamma$ multiplicities, total and average $\gamma$ energy are at the upper end of the experimental data range. Table IV compares the number of $\gamma$ rays for various energy intervals obtained through calculation and measured by Verbinski *et al.* [43]. About 70% of the higher calculated average $\gamma$ multiplicity is due to low energy $\gamma$ rays with an energy of less than 0.5 MeV. In addition, in some cases in our calculations, the sequence of decays in the continuum leads to a residual high-spin state at relatively low energy, just above the discrete level region. When this happens, our calculation tends to over predict the number of $\gamma$ cascades needed to reach a suitable lower excited discrete level, hence producing spurious $\gamma$ transitions and increasing the $\gamma$ multiplicity at the lowest outgoing energies. Our results should therefore be considered valid only above about 100 keV outgoing $\gamma$-ray energy.

The average $\gamma$ multiplicity was calculated as a function of the preneutron emission fragment mass (Fig. 11) considering the three cases of $B = 12\hbar$, $B(A)$, and $B(T, A, \beta)$ for the spin

TABLE IV. The number of $\gamma$ rays for various energy intervals for $n_{th} + {}^{235}$U obtained by Monte Carlo Hauser-Feshbach (MCHF) calculations using $B(T, A, \beta)$ and measured by Verbinski *et al.* [43].

| Energy range | $\gamma$ rays/fission | | | |
|---|---|---|---|---|
| (MeV) | MCHF | Verbinski *et al.* [43] | Difference | |
| 0.14–0.3 | 1.603 | 0.833 | 0.770 | (92.4%) |
| 0.3–0.5 | 1.484 | 1.318 | 0.166 | (12.6%) |
| 0.5–0.7 | 1.192 | 1.182 | 0.010 | (0.8%) |
| 0.7–1.0 | 1.197 | 1.191 | 0.006 | (0.5%) |
| 1.0–1.5 | 1.248 | 1.072 | 0.176 | (16.4%) |
| 1.5–2.0 | 0.611 | 0.461 | 0.150 | (32.5%) |
| 2.0–2.5 | 0.325 | 0.258 | 0.067 | (26.0%) |
| 2.5–3.0 | 0.194 | 0.158 | 0.036 | (22.8%) |
| 3.0–4.0 | 0.139 | 0.143 | −0.004 | (−2.8%) |
| 4.0–5.0 | 0.037 | 0.050 | −0.013 | (−26.0%) |
| 5.0–6.0 | 0.014 | 0.021 | −0.007 | (−33.3%) |
| 6.0–7.0 | 0.0023 | 0.0098 | −0.0075 | (−76.2%) |
| 7.0–10.0 | 0.0006 | 0.0027 | −0.0021 | (−77.2%) |
| 0.14–10.0 | 8.050 | 6.700 | 1.349 | (20.1%) |

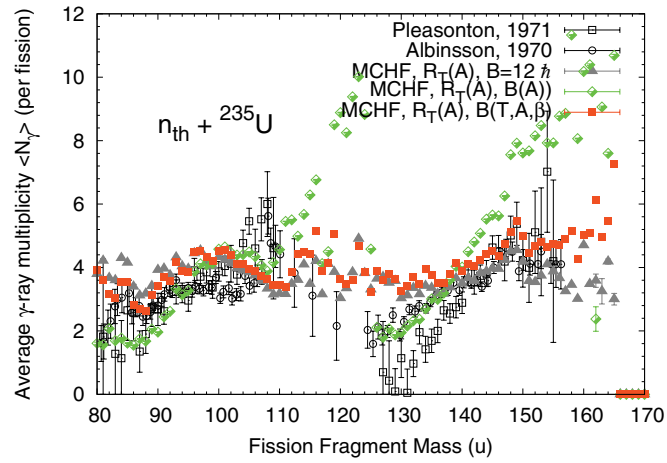


FIG. 11. (Color online) Average prompt fission $\gamma$ multiplicity for $n_{th} + {}^{235}$U as a function of the fragment mass. A constant value spin cut-off parameter $B = 12\hbar$ as well as temperature, mass and ground state deformation dependent spin cut-off parameter $B$ was used in the Monte Carlo Hauser Feshbach (MCHF) calculations. Experimental values are taken from Pleasonton *et al.* [42] and Albinsson *et al.* [45].

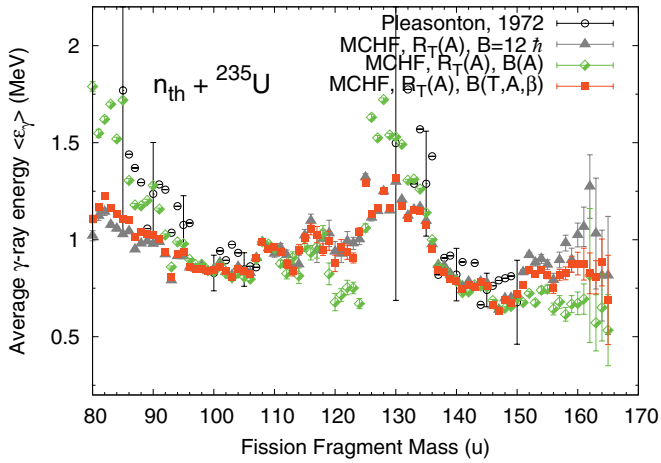


FIG. 12. (Color online) Average $\gamma$ energy for $n_{\rm th} + {}^{235}$U as a function of the fragment mass. A constant value spin cut-off parameter $B = 12\hbar$ as well as temperature, mass and ground state deformation dependent spin cut-off parameter $B$ was used in the Monte Carlo Hauser-Feshbach (MCHF) calculations. Experimental values are taken from Pleasonton *et al.* [42]. Experimental sample error bars are shown at 5-u intervals.

cut-off parameter. Using a constant spin cut-off or $B(T, A, \beta)$ leads to relatively similar results. A relatively good agreement with the data measured by Pleasonton *et al.* [42] and Albinsson *et al.* [45] was obtained with exception of the 120 to 135 u mass region where the calculated multiplicity is significantly higher than the experimental data. A saw-tooth like spin cut-off parameter clearly leads to a saw-tooth like $\gamma$ multiplicity. The emission of the heavy fragment was calculated to be slightly higher than measured data. Note that Albinsson *et al.* [45] used a collimator method to measure $N_\gamma(A)$ while Pleasonton *et al.* [42] applied a Doppler anisotropy technique.

The average $\gamma$ energy is compared to experimental data of Pleasonton *et al.* [42] in Fig. 12. An overall good agreement of all calculations with the experimental results is obtained. For very light fragments all calculations are slightly lower that the experiment. As expected, the average $\gamma$-ray energy increases with the temperature of the emitting fragment, as fewer and more separated levels exist with increasing temperature. In this case, the temperature characterizes the low-lying levels of the nucleus.

### D. $\gamma$-multiplicity distribution

The $\gamma$-multiplicity distribution $P(N_\gamma)$ was calculated (Fig. 13) and compared to the negative binomial distribution model of Valentine [46] given by

$$P(N_\gamma) = \begin{pmatrix} \alpha + N_\gamma - 1 \\ N_\gamma \end{pmatrix} p^\alpha (1-p)^{N_\gamma} \qquad (17)$$

with $\alpha = (D_\gamma - 1)^{-1}$ and $p = \alpha/(\alpha + \overline{N}_\gamma)$, where $D_\gamma$ and $\overline{N}_\gamma$ are relative width and average number of prompt $\gamma$ rays, respectively. Valentine's model is a generalization of Brunson's model [51] for the multiplicity distribution of $^{252}$Cf (sf) (cf. Sec. VI B). Through the use of the generalized parameters of averaged $\gamma$ multiplicity $\overline{N}_\gamma$ and relative width

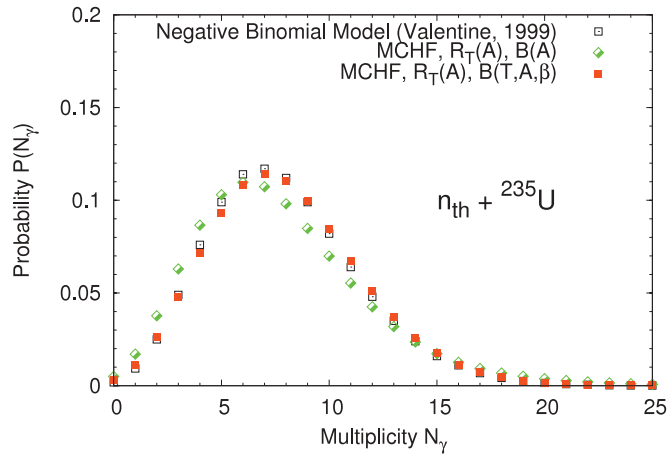


FIG. 13. (Color online) Monte Carlo Hauser-Feshbach model (MCHF) calculation of the $\gamma$ multiplicity distribution for $n_{\rm th} + {}^{235}$U vs. the negative binomial model of Valentine [46] (with $\overline{N}_\gamma = 7.93$ and $D_\gamma = 1.07$).

$D_\gamma$ Valentine's model can be applied for other fissioning systems. The relative widths of the distribution in case of $n_{\rm th} + {}^{235}$U is assumed to be $D_\gamma = 1.07$ [46]. The average neutron multiplicity $\overline{N}_\gamma = 8.05$ is then obtained from the MCHF calculation. The calculated multiplicity distribution is well described by a negative binomial distribution as can be seen in Fig. 13.

### E. Prompt fission $\gamma$ spectrum

The prompt fission $\gamma$ spectrum was calculated using $B(T, A, \beta)$. Figures 14 and 15 compare the MCHF spectrum with experimental results from Verbinski *et al.* [43] and Maienschein *et al.* [52] and with ENDF/B-VII.0 data [33]. All spectra are normalized to their corresponding average $\gamma$ multiplicity.

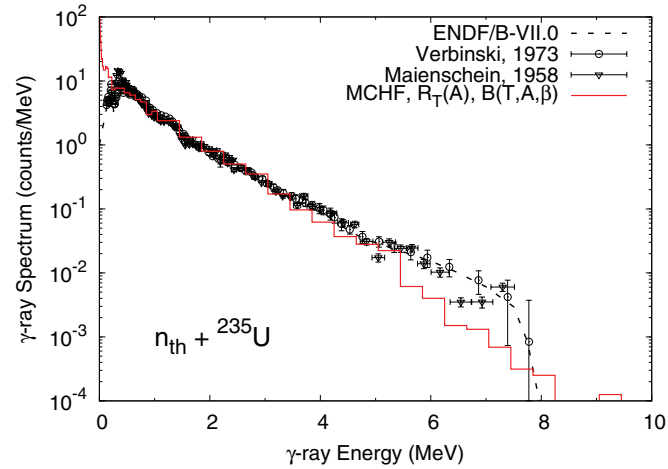


FIG. 14. (Color online) Monte Carlo Hauser-Feshbach model (MCHF) calculation of the prompt fission $\gamma$ spectrum for $n_{\rm th} + {}^{235}$U vs. experimental data of Verbinski *et al.* [43] and Maienschein *et al.* [52] and ENDF/B-VII.0 data [33].

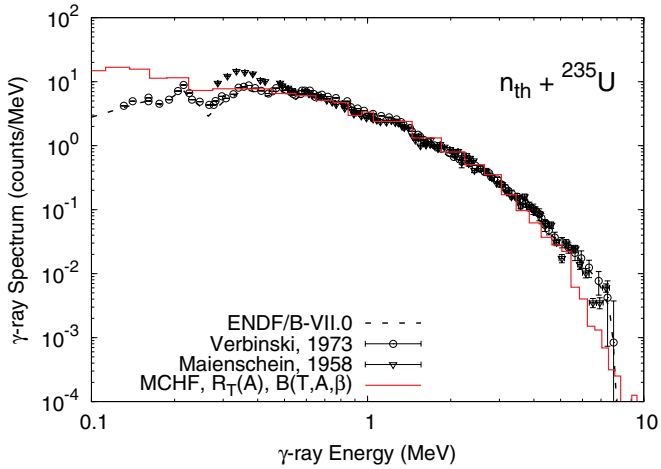


FIG. 15. (Color online) Same as Fig. 14, but plotted in log-log.

In the 0.3–5 MeV energy region, the calculated spectrum is in good agreement with the experiments. At lower energies the calculation overpredicts the number of emitted $\gamma$ rays (see discussion in Sec. IV C). For energies greater than 5 MeV, the MCHF calculation drops off faster than the experimental data.

## V. RESULTS FOR $n_{\text{th}} + {}^{239}\text{Pu}$

Similar calculations were performed for the thermal neutron induced fission of $^{239}$Pu. For all calculations either a temperature, mass and ground state deformation dependent spin cut-off parameter $B(T, A, \beta)$ or a saw-tooth like parameter $B(A)$ in the sampling of the initial fission fragment spin was considered. In case of $B(A)$, we used the same distribution as for $n_{\text{th}} + {}^{235}\text{U}$.

### A. Neutron emission for $n_{\text{th}} + {}^{239}\text{Pu}$

The average neutron multiplicity and center-of-mass energy were calculated as function of the fission fragment mass and are presented in Figs. 16 and 17. The average neutron multiplicity is in good agreement with the experimental data which can be expected since the $R_T$ was chosen by using the ratio $\overline{\nu}_l/\overline{\nu}_h$ (see Sec. III C). Some deviations can be observed for very asymmetric splits ($A_h > 145$) where experimental uncertainties are large. The calculated center-of-mass energy is within the range of the experimental data for both the light and heavy fragments, although specific experimental structures are not reproduced in our calculations.

The neutron multiplicity distributions $P(\nu)$, shown in Fig. 18, was found to be in very good agreement with the experimental data of Holden and Zucker [39].

Figure 19 shows the prompt fission neutron spectrum in the laboratory frame of reference as ratio to a Maxwellian with temperature $T = 1.42$ MeV. For comparison the ENDF/B-VII.0 [33] spectrum as well as several experimental data are

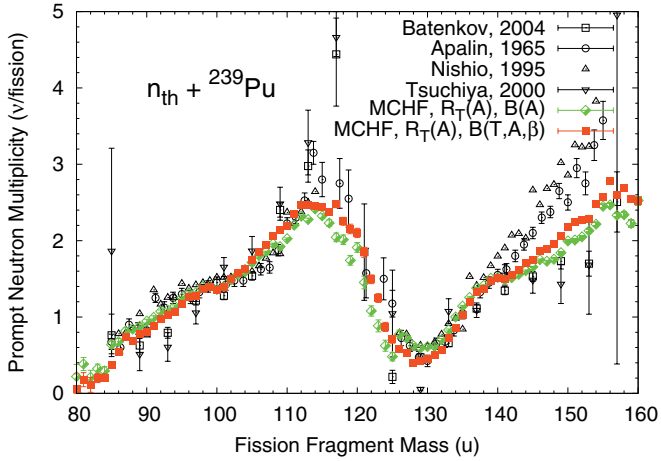


FIG. 16. (Color online) Monte Carlo Hauser-Feshbach model (MCHF) calculations of of the average prompt fission neutron multiplicity for $n_{\text{th}} + {}^{239}$Pu as a function of the fragment mass. Experimental values are taken from Batenkov [35], Apalin [53], Nishio [23], and Tsuchiya [54].

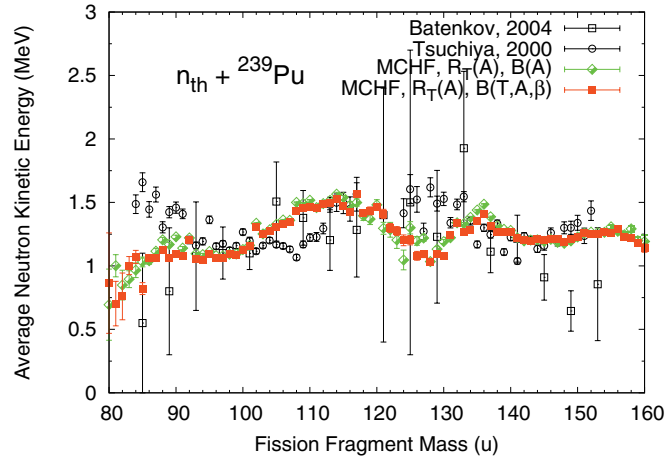


FIG. 17. (Color online) Monte Carlo Hauser-Feshbach model (MCHF) calculations of the average center-of-mass energy of the prompt fission neutrons vs. experimental values of Batenkov [35] and Tsuchiya [54] for $n_{\text{th}} + {}^{239}$Pu.

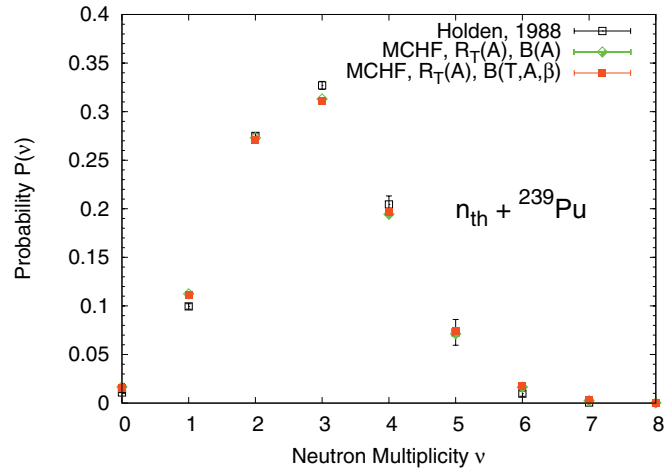


FIG. 18. (Color online) Monte Carlo Hauser-Feshbach model (MCHF) calculations of the neutron multiplicity distribution for $n_{\text{th}} + {}^{239}$Pu compared to the evaluation based on experimental data of Holden and Zucker [39].

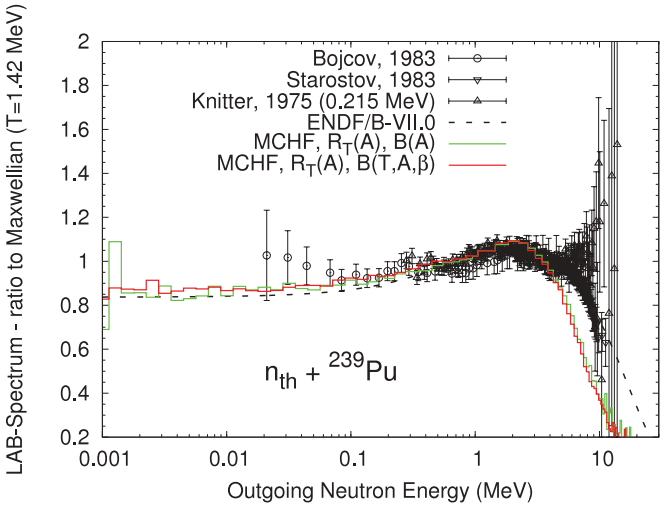


FIG. 19. (Color online) Monte Carlo Hauser-Feshbach model (MCHF) calculation of the average prompt fission neutron spectrum for $n_{\rm th} + {}^{239}$Pu in ratio to a Maxwellian with temperature $T =$ 1.42 MeV. Results are compared to the ENDF/B-VII.0 evaluation [33], as well as experimental data by Bojcov [55], Starostov [56], and Knitter [57].

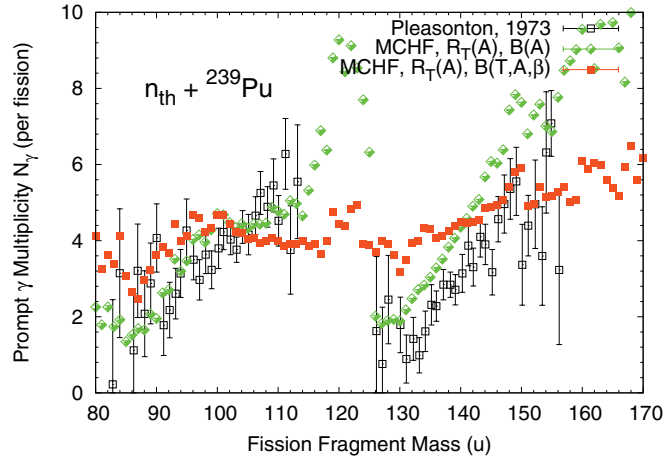


FIG. 20. (Color online) Average prompt fission $\gamma$ multiplicity for $n_{\rm th} + {}^{239}$Pu as a function of the fragment mass. Results of the Monte Carlo Hauser-Feshbach (MCHF) calculations are compared to experimental values from Pleasonton [58].

plotted. All measurements were normalized to the ENDF/B-VII.0 spectrum. The low-energy part of the calculated spectra are close to the ENDF/B-VII.0 spectrum. The high-energy part of the spectra however are much softer than the evaluated spectrum as already observed in the case for $n_{\rm th} + {}^{235}$U.

### B. $\gamma$ emission for $n_{\rm th} + {}^{239}$Pu

The average $\gamma$ multiplicity ($\overline{N}_\gamma$), average $\gamma$ energy ($\overline{\epsilon}_\gamma$), and average total $\gamma$ energy ($\overline{E}_\gamma$) were calculated using a $\gamma$ threshold of 140 keV and the results are summarized in Table V. While the average $\gamma$ energy is in relatively good agreement with the experimental data of Pleasonton [58] and Verbinski *et al.* [43], our MCHF calculations predict too many $\gamma$ rays and therefore over predicts $\overline{E}_\gamma$. Even though using the same lower $\gamma$ energy threshold as Verbinski *et al.* [43] the calculated $\overline{N}_\gamma$ values are by about one $\gamma$ emission higher than found in the experiment.

Figure 20 shows the average prompt fission $\gamma$ multiplicity as a function of the fission fragment mass. Similar to $n_{\rm th} + {}^{235}$U, a pronounced saw-tooth like behavior is found in case of a saw-tooth like spin-cut off parameter $B(A)$. The calculation is in good agreement with the experimental data of Pleasonton [58] for the light fragment but overpredicts $\langle N_\gamma \rangle(A)$ for the heavy one. In case of $B(T, A, \beta)$ the agreement with the experimental data is not as good. Thus, in the 120–140 u mass region the calculated $\overline{N}_\gamma$ is higher and the overall behavior does not follow a saw-tooth form.

Figure 21 shows the calculated average prompt fission $\gamma$ energy as function of the heavy fission fragment mass in comparison to the experimental data of Pleasonton [58]. While the shape of $\overline{\epsilon}_\gamma$ is in reasonable agreement with the data, MCHF-calculated values tend to lie lower than the experimental data.

The calculated $\gamma$ spectrum is shown in Fig. 22 in comparison to the measured spectrum of Verbinski *et al.* [43] and to ENDF/B-VII.0 data [33]. All spectra are normalized to $\overline{N}_\gamma$.

TABLE V. Average $\gamma$ multiplicity ($\overline{N}_\gamma$), average $\gamma$ energy ($\overline{\epsilon}_\gamma$), and total $\gamma$ energy ($\overline{E}_\gamma$) for $n_{\rm th} + {}^{239}$Pu. Monte Carlo Hauser-Feshbach (MCHF) calculations were obtained with a temperature, mass, and ground state deformation dependent spin cut-off parameter $B(T, A, \beta)$. $\Delta E$ is the considered $\gamma$ energy range.

| | $B$ | $\Delta E$ (MeV) | $\overline{N}_\gamma$ [$\gamma$/fission] | $\overline{\epsilon}_\gamma$ [MeV/$\gamma$] | $\overline{E}_\gamma$ [MeV/fission] |
|---|---|---|---|---|---|
| MCHF | $B(A)$ | >0.14 | 8.47 | 0.90 | 7.62 |
| MCHF | $B(T, A, \beta)$ | >0.14 | 8.62 | 0.89 | 7.67 |
| Pleasonton [58] | | >0.085[a] | $6.88 \pm 0.35$ | $0.98 \pm 0.07$ | $6.73 \pm 0.35$ |
| Verbinski *et al.* [43] | | 0.140–10.0 | $7.23 \pm 0.3$ | $0.94 \pm 0.04$ | $6.81 \pm 0.3$ |
| ENDF/B-VII.0 [33] | | | 7.7833 | | |
| ENDF/B-VI.8 | | | 8.095 | | |
| JENDL-4.0 [49] | | | 8.3389 | | |

[a]energy threshold taken from Ref. [51].

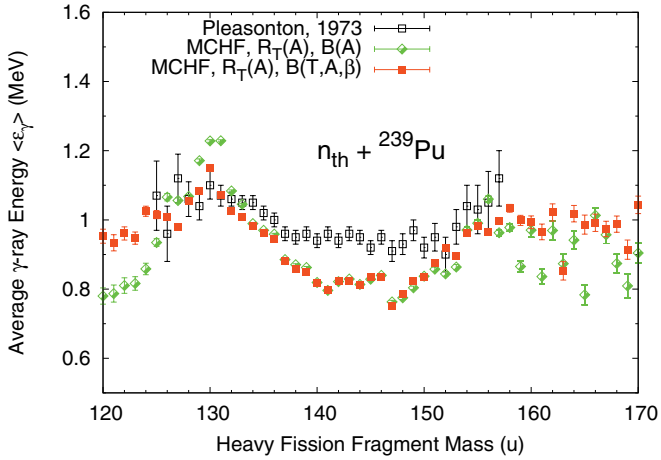


FIG. 21. (Color online) Average prompt fission $\gamma$ energy for $n_{\text{th}} + {}^{239}$Pu as a function of the heavy fragment mass. Results of the Monte Carlo Hauser-Feshbach (MCHF) calculations are compared to experimental values from Pleasonton [58].

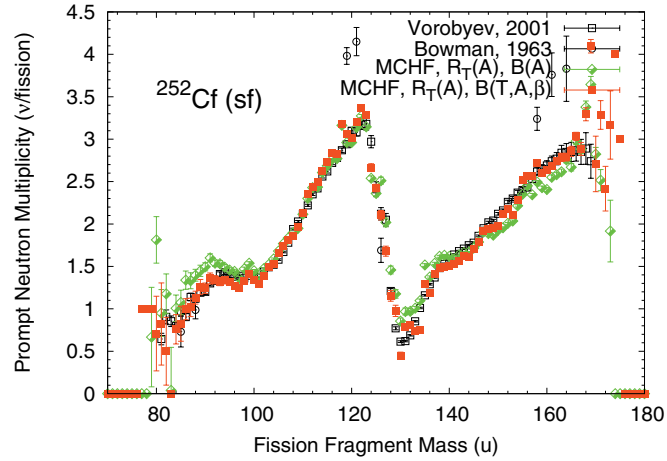


FIG. 23. (Color online) Monte Carlo Hauser-Feshbach model (MCHF) calculations of the average prompt fission neutron multiplicity for $^{252}$Cf (sf) as a function of the fragment mass. Experimental values are taken from Vorobyev *et al.* [59] and Bowman *et al.* [61].

Similar to the $n_{\text{th}} + {}^{235}$U case, the calculated spectrum is higher than the experiment and ENDF/B-VII.0 for the lower energy part of the spectrum. In the fast energy region the calculated spectrum is slightly lower.

## VI. RESULTS FOR $^{252}$Cf (sf)

### A. Neutron emission for $^{252}$Cf (sf)

Due to fact that we chose the excitation energy sharing according to the best agreement with the experimental ratio $\nu_l/\nu_h$, the average neutron emission as function of fragment mass [$\overline{\nu}(A)$] is very well reproduced as shown in Fig. 23. The calculated average neutron kinetic energy as function of the fragment mass is in good agreement with the experimental data in case of the light fragment (Fig. 24). For the heavy fragment the calculation is to some extent lower. In addition, one has to note that in particular for symmetric mass splits the discrepancy of the experimental data is quite large. Inferring an average neutron kinetic energy in the center-of-mass from experimental data requires the use of several important assumptions that can lead to important systematic biases. We are currently investigating this issue to better understand the reason for this discrepancy. However, a too low calculated average energy is also reflected in the spectrum observed in Fig. 25, which may indicate a problem with the calculations as well.

The calculated neutron spectrum is compared to experimental data and the ENDF/B-VII.0 [33] spectrum as ratio to a Maxwellian with $T = 1.42$ MeV (Fig. 25). All experimental data have been normalized to the ENDF/B-VII.0 spectrum. In contrast to the result for $n_{\text{th}} + {}^{235}$U and $n_{\text{th}} + {}^{239}$Pu, in this case

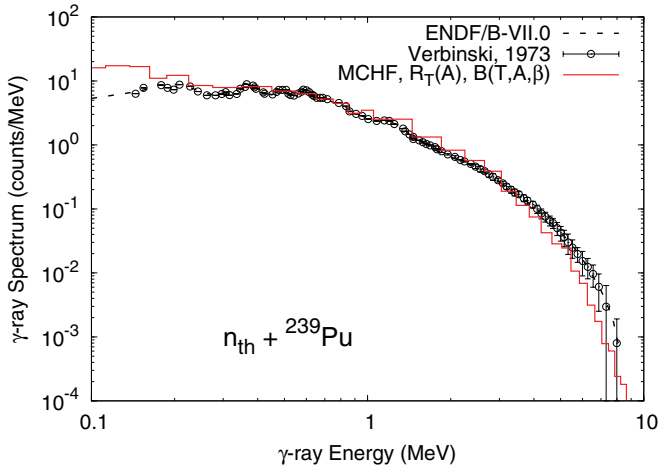


FIG. 22. (Color online) Monte Carlo Hauser-Feshbach model (MCHF) calculation of the prompt fission $\gamma$ spectrum for $n_{\text{th}} + {}^{239}$Pu compared to experimental data of Verbinski *et al.* [43] and to the ENDF/B-VII.0 evaluation [33].

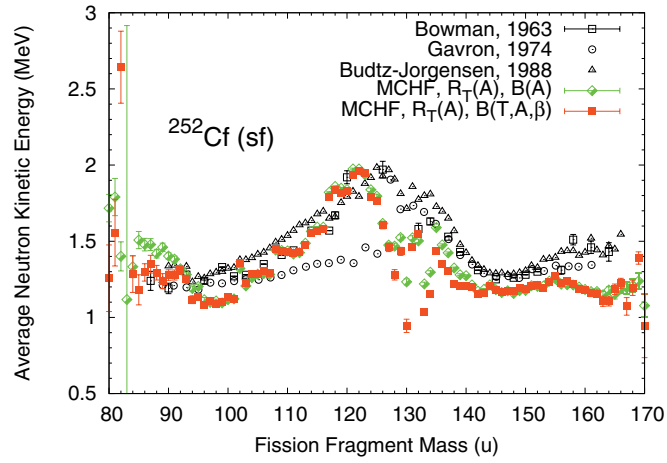


FIG. 24. (Color online) Monte Carlo Hauser-Feshbach model (MCHF) calculations of the average center-of-mass energy of the prompt fission neutrons for $^{252}$Cf (sf). Experimental data are taken from Bowman *et al.* [61], Gavron *et al.* [62], and Budtz-Jorgensen *et al.* [63].

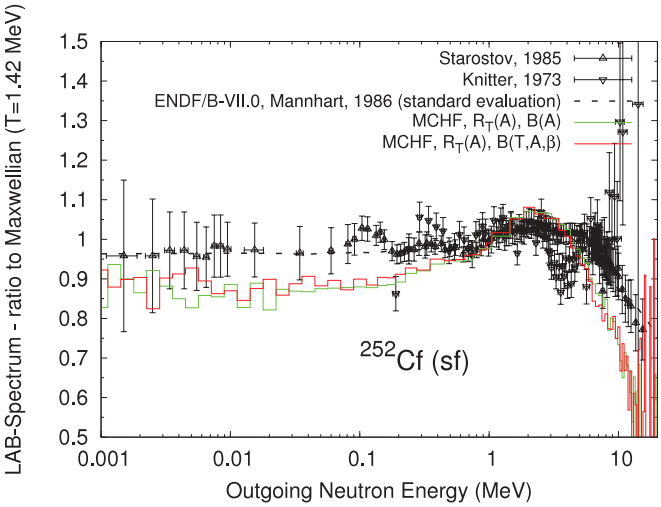


FIG. 25. (Color online) Monte Carlo Hauser-Feshbach model (MCHF) calculations of the average prompt fission neutron spectrum for $^{252}$Cf (sf) in ratio to a Maxwellian with temperature $T = 1.42$ MeV. The calculation are compared to the standard evaluation of Mannhart [64] used by ENDF/B-VII.0 [33] and experimental data from Starostov *et al.* [65] and Knitter *et al.* [66].

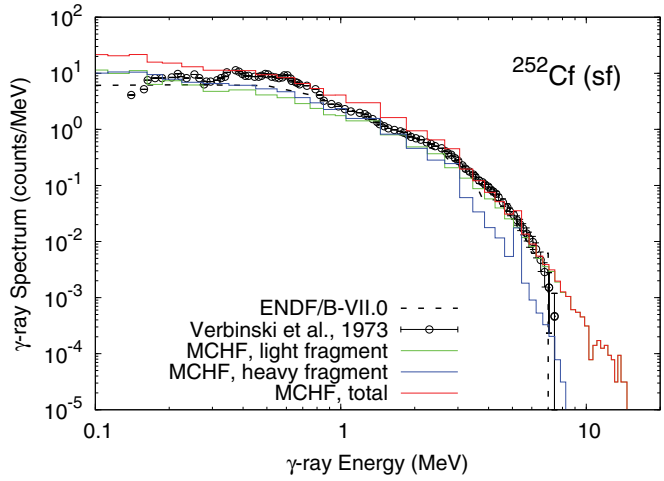


FIG. 26. (Color online) Monte Carlo Hauser-Feshbach model (MCHF) calculation of the average prompt fission $\gamma$ spectrum for $^{252}$Cf (sf) compared to experimental data of Verbinski *et al.* [43] and to ENDF/B-VII.0 data [33].

the low energy tail of the spectrum is underpredicted by the calculation. For the fast part of the spectrum we find a similar trend as for the other two systems,which is a softer spectrum compared to ENDF/B-VII.0 and the experimental data.

### B. $\gamma$ emission for $^{252}$Cf (sf)

The average properties of the $\gamma$ emission from spontaneous fission of $^{252}$Cf are summarized in Table VI. The average $\gamma$ multiplicity in both calculations are substantially higher than the experimental data by about 1–2 $\gamma$ rays per fission. Comparing the calculated $\gamma$ spectrum to measurements of Verbinski *et al.* [43] (Fig. 26) one can note that this is mainly due to an increased number of $\gamma$ rays predicted with energy of 0.8–4 MeV and less than 0.4 MeV.

Figure 27 shows the average $\gamma$-ray multiplicity as function of the fission fragment mass. As for $n_{\text{th}} + ^{235}$U, both initial spin models lead to a saw-tooth behavior for the $\gamma$ multiplicity. Some deviation between both calculations can be noticed in the 125–140 u mass region. For the $\gamma$ emission from the light fragment our calculations are reasonable agreement with all the experimental data. For the heavy fragment however, the calculations are only in agreement with the data of Johansson [70]. Data from Pleasonton *et al.* [67] and MPI [71] are lower than the calculation, in particular for masses higher than 140 u.

Figure 28 shows a comparison of the calculated $\gamma$ multiplicity distribution with Brunson's model [51]. Brunson used a double Poisson function to fit experimental multiplicity

TABLE VI. Average $\gamma$ multiplicity ($\overline{N}_\gamma$), average $\gamma$ energy ($\overline{\epsilon}_\gamma$), and total $\gamma$ energy ($\overline{E}_\gamma$) for $^{252}$Cf (sf). Monte Carlo Hauser-Feshbach (MCHF) calculations were done with a temperature, mass, and deformation dependent spin cut-off parameter $B(T, A, \beta)$ and a saw-tooth like spin cut-off parameter $B(A)$. $\Delta E$ is the considered $\gamma$ energy range.

| | $B$ | $\Delta E$ (MeV) | $\overline{N}_\gamma$ [$\gamma$/fission] | $\overline{\epsilon}_\gamma$ [MeV/$\gamma$] | $\overline{E}_\gamma$ [MeV/fission] |
|---|---|---|---|---|---|
| MCHF | $B(A)$ | >0.14 | 9.97 | 0.85 | 8.47 |
| MCHF | $B(T, A, \beta)$ | >0.14 | 10.7 | 0.85 | 9.10 |
| Skarsvåg [68] | | >0.114 | $9.7 \pm 0.4$ | 0.72 | $7.0 \pm 0.3$ |
| Pleasonton *et al.* [67] | | >0.085[a] | $8.32 \pm 0.4$ | $0.85 \pm 0.06$ | $7.06 \pm 0.35$ |
| Smith *et al.* [60] | | >0.040[a] | 10.3 | 0.80 | 8.2 |
| Verbinski *et al.* [43] | | 0.140–10.0 | $7.80 \pm 0.3$ | $0.88 \pm 0.04$ | $6.84 \pm 0.3$ |
| Bowman and Thompson [44] | | >0.040[a] | 10. | $0.90 \pm 0.06$ | 8.6 |
| Val'skii *et al.* [69] | | >0.100[a] | $7.5 \pm 1.5$ | $0.96 \pm 0.08$ | 7.2 |
| Brunson [51] | | >0.085 | 8.32 | | |
| Brunson [51] | | >0.140 | 7.8 | | |
| ENDF/B-VII.0 [33] | | | 7.7833 | | |
| JENDL4.0 [49] | | | 8.3389 | | |

[a]energy threshold taken from [51].

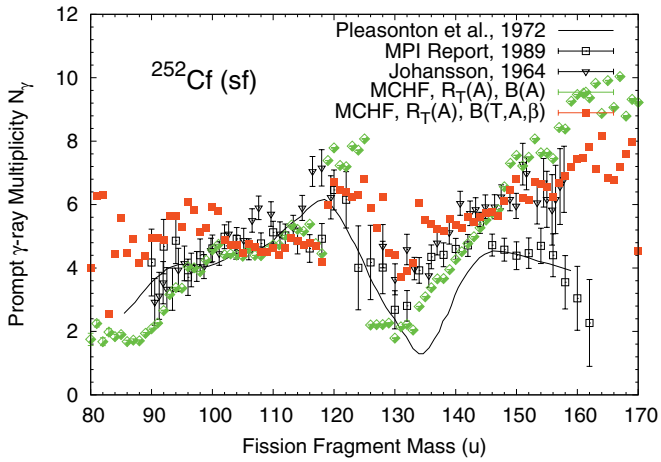


FIG. 27. (Color online) Average prompt fission $\gamma$ multiplicity for $^{252}$Cf (sf) as a function of the fragment mass. Results of the Monte Carlo Hauser-Feshbach (MCHF) calculations are compared to experimental values from Johansson [70] and MPI [71] and from Pleasonton *et al.* [67].

distributions. Since Brunson's average $\gamma$ multiplicity is smaller than the MCHF result (see Table VI), the obtained MCHF multiplicity distributions are significantly broader. Additionally, Valentine's negative binomial model [46] is plotted using $\overline{N}_\gamma$ from MCHF calculations and input into Eq. (17). Using the the same value for $\overline{N}_\gamma$ in Valentine's model as obtained in the calculation the multiplicity distribution is well described by the negative binomial function.

## VII. DISCUSSION

In the presented MCHF study of the neutron and $\gamma$ emission from fission of $n_{\rm th} + ^{235}$U, $n_{\rm th} + ^{239}$Pu, and $^{252}$Cf (sf) two major components are free parameters that impact valuable information about the postscission fragment characteristics namely the excitation energy sharing between the light and the heavy

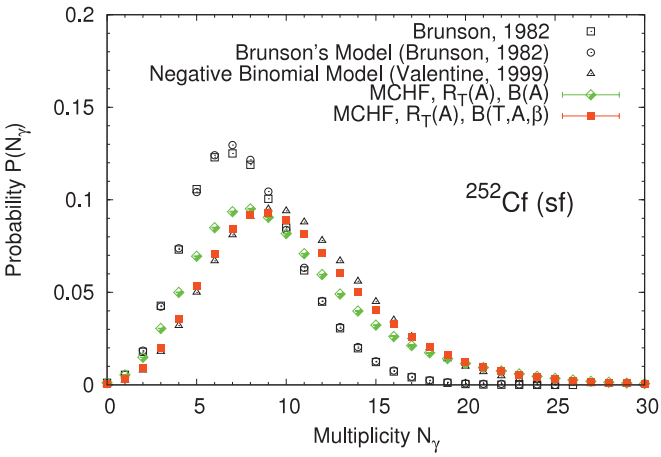


FIG. 28. (Color online) Monte Carlo Hauser-Feshbach model (MCHF) calculation of the $\gamma$ multiplicity distribution for $^{252}$Cf (sf) compared to experimental data from Brunson [51], Brunson's Model [51], and to the negative binomial model of Valentine [46] (with $\overline{N}_\gamma = 10.5$ and $D_\gamma = 1.074$).

fragment and the initial fission fragment spin distribution. As discussed in several publications (e.g., [6,7,22]) the excitation energy sharing can be obtained through a study of the neutron emission ratio ratio $\overline{\nu}_l/\overline{\nu}_h$.

The initial spin distribution influences strongly the neutron-$\gamma$ competition and the average neutron multiplicity $\overline{\nu}$ as well as the average $\gamma$ emission as function of mass $N_\gamma(A)$. In order to obtain the best agreement of the simulations with the available experimental data set, two trends were observed common to all three studied systems: (i) The initial fission fragment spin is found to be significantly higher than values inferred from isomeric ratio measurements. An average initial spin $J_{\rm rms}$ of about $12\hbar$ leads to a reasonable agreement of the calculated and experimental values for the neutron multiplicity. (ii) Including a mass dependence of the initial spin distribution rather than an average value improves significantly the agreement of the calculated average $\gamma$ multiplicity as function of mass with experimental results. However, one has to note that the experimental and theoretical knowledge regarding the initial fission fragment spin distribution is quite ambiguous as discussed in detail by Piasecki and Blocki [72]. While isomeric measurements tend to result in lower fragment spin distributions, results based on $\gamma$ anisotropy, the $\gamma$ de-excitation in general, or based on theoretical models may result in lower or higher spin distributions than the one assumed in this work.

We have started comparing calculated isomeric yield ratios with measured data, instead of the initial spin in order to be independent of the model used by experimentalist to deduce the initial spin from isomeric yield ratios. The information of isomeric ratios is in principle available in our calculations. Comparing these with experimental values will improve the comparison and help to identify more clearly differences. In addition, to our knowledge there are only a few measurements of the average $\gamma$ multiplicity as function of mass available for the three studied systems, mainly from Pleasonton *et al.* [42,58,67]. New measurements of the $\gamma$ multiplicity are highly desirable. In addition, the model of the moment of inertia should be extended to include a possible excitation energy dependence.

Two additional general trends were observed throughout the study. The high-energy tail of the neutron spectrum is consistently softer compared to the ENDF/B-VII.0 spectrum and experiments, which remains puzzling. The $\gamma$ multiplicity is higher than experimental results due to an increased number of low energy $\gamma$ rays. A detailed study of the calculation sensitivity to the used spin dependent level densities as well as calculations considering a non-isotropic neutron emission could help shed some light on these issues.

At this stage of the development the coupling the CGM and FFD codes leads to a significant increase of the runtime compared to the MCW calculations. However, by merging the two codes and the use of parallelization the runtime could be reduced.

## VIII. CONCLUSION

In this paper, calculations of the prompt $\gamma$ and neutron emission from primary fission fragments were presented using a Monte Carlo Hauser-Feshbach approach by coupling the

CGM and FFD codes. Three different systems were studied: $n_{th} + {}^{235}U$, $n_{th} + {}^{239}Pu$, and ${}^{252}Cf$ (sf). The overall agreement of the calculated $\gamma$ and neutron characteristics with available experimental data was found to be good. Some differences were identified for the $\gamma$ multiplicity and the fast part of the neutron spectrum in the laboratory frame. The initial spin distribution of the fission fragments was found to be one of the most important input quantities since it directly impacts the neutron-$\gamma$ competition. The sensitivity of MCHF calculations to the initial spin distribution was studied. The use of a saw-tooth like initial spin distribution lead to the best agreement of the calculated average $\gamma$ multiplicity as function of mass.

In a future work, a more detailed sensitivity study regarding the various input parameters, such as the primary fission fragment yield, the initial spin distribution and level density formalism could improve the calculation by estimating the overall uncertainty of the results. A calculation of isomer ratios will be performed in order to make a direct comparison with measured data.

## ACKNOWLEDGMENTS

We would like to thank R. Vogt (LLNL), J. Randrup (LBNL), O. Litaize, O. Serot, and D. Regnier (CEA Cadarache), M. B. Chadwick, M. Jandel, and J. Ullmann (LANL) for helpful and stimulating discussions. This work was supported in part by the AFCI Nuclear Energy University Program (DE-AC07-05ID14517 subcontract no. 00091100). It was performed in part under the auspices of the National Nuclear Security Administration of the US Department of Energy at Los Alamos National Laboratory under Contract No. DE-AC52-06NA25396.

[1] J. C. Browne and F. S. Dietrich, Phys. Rev. C **10**, 2545 (1974).
[2] S. Lemaire, P. Talou, T. Kawano, M. B. Chadwick, and D. G. Madland, Phys. Rev. C **72**, 024601 (2005).
[3] S. Lemaire, P. Talou, T. Kawano, M. B. Chadwick, and D. G. Madland, Phys. Rev. C **73**, 014602 (2006).
[4] J. Randrup and R. Vogt, Phys. Rev. C **80**, 024601 (2009).
[5] R. Vogt, J. Randrup, J. Pruet, and W. Younes, Phys. Rev. C **80**, 044611 (2009).
[6] O. Litaize and O. Serot, Phys. Rev. C **82**, 054616 (2010).
[7] P. Talou, B. Becker, T. Kawano, M. B. Chadwick, and Y. Danon, Phys. Rev. C **83**, 064612 (2011).
[8] R. Vogt, J. Randrup, D. A. Brown, M. A. Descalle, and W. E. Ormand, Phys. Rev. C **85**, 024608 (2012).
[9] T. Kawano, P. Talou, M. B. Chadwick, and T. Watanabe, J. Nucl. Sci. Technol. **47**, 462 (2010).
[10] V. Weisskopf, Phys. Rev. **52**, 295 (1937).
[11] W. Hauser and H. Feshbach, Phys. Rev. **87**, 366 (1952).
[12] T. Kawano, P. Talou, and M. B. Chadwick, EPJ Web Conferences **21**, 04001 (2012).
[13] A. J. Koning and J. P. Delaroche, Nucl. Phys. A **713**, 231 (2003).
[14] R. Capote *et al.*, Nucl. Data Sheets **110**, 3107 (2009).
[15] A. Gilbert and A. G. W. Cameron, Can. J. Phys. **43**, 1446 (1965).
[16] C. Romano, Y. Danon, R. Block, J. Thompson, E. Blain, and E. Bond, Phys. Rev. C **81**, 014607 (2010).
[17] F.-J. Hambsch (personal communication).
[18] "Systematics of Fission-Product Yields," A. C. Wahl, LANL Report No. LA-13928 (2002).
[19] T. Ohsawa and T. Shibata, in *Proceedings of the International Conference on Nuclear Data for Science and Technology*, Julich, Germany, Research Reports in Physics, edited by S. M. Qaim (Springer-Verlag, Berlin, 1991), p. 965.
[20] D. G. Madland and J. R. Nix, Nucl. Sci. Eng. **81**, 213 (1982).
[21] P. Möller, J. R. Nix, W. D. Myers, and W. J. Swiatecki, At. Data Nucl. Data Tables **59**, 185 (1995).
[22] C. Manailescu, A. Tudora, F.-J. Hambsch, C. Morariu, and S. Oberstedt, Nucl. Phys. A **867**, 12 (2011).
[23] K. Nishio, Y. Nakagome, H. Yamamoto, and I. Kimura, Nucl. Phys. A **632**, 540 (1998).
[24] A. S. Vorobyev, O. A. Shcherbakov, Yu. S. Pleva, A. M. Gagarski, G. V. Val'ski, G. A. Petrov, V. I. Petrova, and T. A. Zavarukhina, in *Proceedings of ISINN-17*, Dubna, Russia, May 27–30 (Joint Institute of Nuclear Research, Dubna, 2009).
[25] G. Mouze, C. Ythier, and S. Hachem, arXiv:1103.5341v1 (2011); original data from J. L. Durell, in *Proceedings of the Third International Conference on Dynamical Aspects of Nuclear Fission*, Casta Papiernicka, Slovakia, Aug. 30–Sep. 4, 1996, edited by J. Kliman and B. l. Pustylnik (J.I.N.R., Dubna, 1996), p. 270.
[26] T. Ericson, Adv. Phys. **9**, 425 (1960).
[27] G. Audi, A. H. Wapstra, and C. Thibault, Nucl. Phys. A **729**, 337 (2003).
[28] D. C. Aumann, W. Gückel, E. Nirschl, and H. Zeising, Phys. Rev. C **16**, 254 (1977).
[29] H. Naik, S. P. Dange, R. J. Singh, and T. Datta, Nucl. Phys. A **587**, 273 (1995).
[30] N. E. Holden, in *Proceedings of the International Conference on Nuclear Data for Science and Technology*, Mito (Saikon Publishing, Tokyo, 1988), p. 795.
[31] J. C. Hopkins and B. C. Diven, Nucl. Phys. **48**, 433 (1963).
[32] H.-Q. Zhang, Inst. At. Energy, Beijing Reports **76041** (1978); EXFOR No. V0022.002.
[33] M. B. Chadwick *et al.*, Nucl. Data Sheets **107**, 2931 (2006).
[34] E. E. Maslin, A. L. Rodgers, and W. G. F. Core, Phys. Rev. **164**, 1520 (1967).
[35] O. A. Batenkov, G. A. Boykov, F.-J. Hambsch, J. H. Hamilton, V. A. Jakovlev, V. A. Kalinin, A. B. Laptev, V. E. Sokolov, and A. S. Vorobyev, in *Proceedings of the International Conference on Nuclear Data for Science and Technology ND2004*, Sep. 26–Oct. 1, 2004, Santa Fe, NM, USA, edited by R. C. Haight, M. B. Chadwick, T. Kawano, and P. Talou (AIP, Melville, 2004) [AIP Conf. Proc. **769**, 1003 (2004)].
[36] C. B. Franklyn, C. Hofmeyer, and D. W. Mingay, Phys. Lett. B **78**, 564 (1978).
[37] J. W. Boldeman and A. W. Dalton, AAEC/E172, Australian Atomic Energy Commission, Lucas Heights (1967).
[38] B. C. Diven, H. C. Martin, R. F. Taschek, and J. Terrell, Phys. Rev. **101**, 1012 (1956).
[39] N. E. Holden and M. S. Zucker, Nucl. Sci. Eng. **98**, 174 (1988).

[40] N. Kornilov, F.-J. Hambsch, I. Fabry, S. Oberstedt, T. Belgya, Z. Kis, L. Szentmiklosi, and S. Simakov, Nucl. Sci. Eng. **165**, 117 (2010).
[41] A. S. Vorobyev, O. A. Shcherbakov, A. M. Gagarski, G. V. Val'ski, and G. A. Petrov, EPJ Web of Conferences **8**, 03004 (2010).
[42] F. Pleasonton, R. L. Ferguson, and H. W. Schmitt, Phys. Rev. C **6**, 1023 (1972).
[43] V. V. Verbinski, H. Weber, and R. E. Sund, Phys. Rev. C **7**, 1173 (1973).
[44] H. R. Bowman and S. G. Thompson, in *Proceedings of the Second United Nations International Conference on the Peaceful Uses of Atomic Energy*, Geneva (United Nations, NY, 1958), Vol. 15, p. 212.
[45] H. Albinsson and L. Lindow, Report AE-398, Aktiebolaget Atomenergi Studsvik, Nyköping, Sweden (1970).
[46] T. E. Valentine, ORNL Report No. ORNL/TM-1999/300.
[47] R. W. Peelle and F. C. Maienschein, Phys. Rev. C **3**, 373 (1971).
[48] JEFF Report 21 (2006), edited by A. Koning, R. Forrest, M. Kellett, R. Mills, H. Henriksson, and Y. Rugama.
[49] K. Shibata, O. Iwamoto, T. Nakagawa, N. Iwamoto, A. Ichihara, S. Kunieda, S. Chiba, K. Furutaka, N. Otuka, T. Ohsawa, T. Murata, H. Matsunobu, A. Zukeran, S. Kamada, and J. Katakura, J. Nucl. Sci. Technol. **48**, 1 (2011).
[50] Z. G. Ge, Z. X. Zhao, H. H. Xia, Y. X. Zhuang, T. J. Liu, J. S. Zhang, and H. C. Wu, J. Korean Phys. Soc. **59**, 1052 (2010).
[51] G. S. Brunson, LANL Report LA-9408-T (1982).
[52] F. C. Maienschein, R. W. Peelle, W. Zobel, and T. A Love, *Second United Nations International Conference on the Peaceful Uses of Atomic Energy*, A/CONF.15/P/670 (United Nations, NY, 1958).
[53] V. F. Apalin, Yu. N. Gritsyuk, I. E. Kutikov, V. I. Lebedev, and L. A. Mikaelian, Nucl. Phys. **71**, 553 (1965).
[54] C. Tsuchiya, Y. Nakagome, H. Yamana, H. Moriyama, K. Nishio, I. Kanno, K. Shin, and I. Kimura, J. Nucl. Sci. Technol. **37**, 941 (2000).
[55] A. A. Bojcov, A. F. Semenov, and B. I. Starostov, in *Proceedings of the 6th All Union Conference on Neutron Physics*, Kiev, 2–6 October 1983, p. 294, EXFOR entry 40873-006 (1983).
[56] V. N. Nefedov, B. I. Starostov, and A. A. Boytsov, [55], Vol. 2 (USSR), p. 285, EXFOR entry 40871-006 (1983).
[57] H. H. Knitter, Atomkernenergie **26**, 76 (1975); EXFOR No. 20576.003.
[58] F. Pleasonton, Nucl. Phys. A **213**, 413 (1973).
[59] A. S. Vorobyev, V. N. Dushin, F. J. Hambsch, V. A. Yakovlev, V. A. Kalinin, I. S. Kraev, A. B. Laptev, B. F. Petrov, G. A. Petrov, Y. S. Pleva, O. A. Shcherbakov, and V. E. Sokolov, *IX International Seminar on Interactions of Neutrons with Nuclei*, 288 (Joint Institute of Nuclear Research, Dubna, 2001); V. N. Dushin, F.-J. Hambsch, V. A. Jakovlev, V. A. Kalinin, I. S. Kraev, A. B. Laptev, D. V. Nikolaev, B. F. Petrov, G. A. Petrov, V. I. Petrova, Y. S. Pleva, O. A. Shcherbakov, V. I. Shpakov, V. E. Sokolov, A. S. Vorobyev, and T. A. Zavarukhina, Nucl. Phys. A **516**, 539 (2004).
[60] A. B. Smith, P. R. Fields, and A. M. Friedman, Phys. Rev. **104**, 699 (1956).
[61] H. R. Bowman, J. C. D. Milton, S. G. Thompson, and W. J. Swiatecki, Phys. Rev. **129**, 2133 (1963).
[62] A. Gavron and Z. Fraenkel, Phys. Rev. C **9**, 632 (1974).
[63] C. Budtz-Jørgensen and H.-H. Knitter, Nucl. Phys. A **490**, 307 (1988).
[64] W. Mannhart, IAEA-TECDOC-410 (1986).
[65] B. I. Starostov, V. N. Nefedov, and A. A. Boykov, Vop. At. Nauki i Tekhn., Ser. Yadernye Konstanty **1985**, 16 (1985); USSR report to International Nuclear Data Center **293**, 19 (1989); EXFOR No. 40930-002.
[66] H. H. Knitter, A. Paulsen, H. Liskien, and M. M. Islam, Atomkernenergie **22**, 84 (1973); EXFOR No. 20401.002.
[67] F. Pleasonton, R. L. Ferguson, and H. W. Schmitt, ORNL report 4844 (1972).
[68] K. Skarsvåg, Phys. Rev. C **22**, 638 (1980).
[69] G. V. Valśkii, D. M. Kaminker, G. A. Petrov, and L. A. Popeko, At. Energ. **18**, 3 (1965).
[70] S. A. E. Johansson, Nucl. Phys. **60**, 378 (1964).
[71] R. Schmid-Fabian, Max-Planck-Institut für Kernphysik Heidelberg (MPI), Report MPI H 1989 – V 15 (1989) (in German).
[72] E. Piasecki and J. Blocki, Acta Phys. Pol. B **5**, 247 (1974).